Inorganic Chemistry
Article

Inorg. Chem. **2009**, *48*, 10093–10101 **10093**
DOI: 10.1021/ic900993j

One-Pot, Template Syntheses of a New Class of Metallomacrocycles with a Tetraoxime Cyclic Skeleton

Shohei Tashiro, Ai Minoda, Mihoko Yamada, and Mitsuhiko Shionoya*

Department of Chemistry, Graduate School of Science, The University of Tokyo, 7-3-1 Hongo, Bunkyo-ku, Tokyo 113-0033, Japan

Received May 21, 2009

Most common macrocycles such as crown ethers, porphyrins, and macrocyclic polyamines show versatile, excellent functions in a variety of research fields such as coordination chemistry, supramolecular chemistry, analytical chemistry, and material sciences. Thus, the rational design of a new class of readily synthesized macrocyclic metal ligands is a key to the development of a new category of functionalized macrocyclic metal complexes. Herein, we report one-pot, template syntheses of a new class of metallomacrocycles with a 16-membered tetraoxime cyclic skeleton from a dioxime in the presence of a template transition-metal ion such as Fe^{2+}, Ni^{2+}, Cu^{2+}, Co^{2+}, or Ag^{+}. These metal ions can be easily removed from the mononuclear metallomacrocycles, and, for example, the metal-free tetraoxime ligand was obtained in 90% yield when Fe^{2+} was used as the template. It would appear that this one-pot, metal-template cyclization efficiently proceeds through continual metal-mediated oxime exchange reactions. Interestingly, Pd^{2+}, which does not afford any cyclized products, formed a 1:1 complex with the macrocyclic ligand. The molecular structures of the metal-free ligand, its 1:1 metal complexes with Fe^{2+}, Ni^{2+}, Cu^{2+}, Pd^{2+}, and Ag^{+}, and a dinuclear complex with Ag^{+} were fully determined by single-crystal X-ray analyses. UV−visible absorption spectra and cyclic voltammetry measurements of these complexes are also reported.

Introduction

Macrocyclic metal ligands are widely recognized as functional molecules that can bring out the full potential of accommodated metal ion(s). As shown in a number of excellent examples of universal ligands such as crown ethers,[1] porphyrins,[2] and saturated (or unsaturated) macrocyclic polyamines,[3] their chemical properties and functions as metal complexes have been systematically enhanced by the facile and diversified chemical modification of their macrocyclic frameworks. Hence, the rational design of a new class of macrocyclic ligands and their metal complexes with desirable properties is still a notable achievement.

Among a series of synthetic methods for universal macrocycles reported so far, template-directed synthesis is most frequently used.[4] Additionally, their template syntheses allow easy chemical modification of their macrocyclic skeletons, which would provide a new class of macrocyclic metal complexes possessing unique structures, properties, and functions.

Nitrogen donors are most common among a series of metal-binding sites. Reversible covalent bonds such as imine groups (-C═N-) have widely been used for metal-templated preparation of polyaza macrocyclic[5] or Schiff-base[6] metal complexes. Imine analogs such as the oxime (-C═N−O-) group have also been utilized as a building block for macrocyclic metal complexes. It is more than 100 years ago that a dimethylglyoxime ligand was found to provide a macrocyclic skeleton through hydrogen-bonded dimerization.[7] Since then, a number of excellent

*Corresponding author e-mail: shionoya@chem.s.u-tokyo.ac.jp.

(1) (a) Gokel, G. W.; Leevy, W. M.; Weber, M. E. *Chem. Rev.* **2004**, *104*, 2723–2750. (b) Pedersen, C. J.; Frensdorff, H. K. *Angew. Chem., Int. Ed. Engl.* **1972**, *11*, 16–25. (c) Krakowiak, K. E.; Bradshaw, J. S.; Zamecka-Krakowiak, D. J. *Chem. Rev.* **1989**, *89*, 929–972.

(2) (a) *The Porphyrin Handbook*; Academic Press: San Diego, 2000. (b) Sessler, J. L.; Seidel, D. *Angew. Chem., Int. Ed.* **2003**, *42*, 5134–5175. (c) Hambright, P. *Coord. Chem. Rev.* **1971**, *6*, 247–268.

(3) (a) Kimura, E. *Tetrahedron* **1992**, *48*, 6175–6217. (b) Busch, D. H. *Acc. Chem. Res.* **1978**, *11*, 392–400. (c) Busch, D. H. *Chem. Rev.* **1993**, *93*, 847–860. (d) Christensen, J. J.; Eatough, D. J.; Izatt, R. M. *Chem. Rev.* **1974**, *74*, 351–384. (e) Izatt, R. M.; Bradshaw, J. S.; Nielsen, S. A.; Lamb, J. D.; Christensen, J. J.; Sen, D. *Chem. Rev.* **1985**, *85*, 271–339. (f) Izatt, R. M.; Pawlak, K.; Bradshaw, J. S.; Bruening, R. L. *Chem. Rev.* **1991**, *91*, 1721–2085. (g) Izatt, R. M.; Bradshaw, J. S.; Pawlak, K.; Bruening, R. L.; Tarbet, B. J. *Chem. Rev.* **1992**, *92*, 1261–1354. (h) Izatt, R. M.; Pawlak, K.; Bradshaw, J. S. *Chem. Rev.* **1995**, *95*, 2529–2586. (i) Zhang, X. X.; Bradshaw, J. S.; Izatt, R. M. *Chem. Rev.* **1997**, *97*, 3313–3361. (j) Lehn, J.-M. *Angew. Chem., Int. Ed. Engl.* **1988**, *27*, 89–112.

(4) (a) Costisor, O.; Linert, W. *Metal Mediated Template Synthesis of Ligands*; World Scientific Publishing Co. Pte. Ltd.: Singapore, 2004. (b) Greene, R. N. *Tetrahedron Lett.* **1972**, *13*, 1793–1796. (c) Bradshaw, J. S.; Stott, P. E. *Tetrahedron* **1980**, *36*, 461–510. (d) Jasat, A.; Dolphin, D. *Chem. Rev.* **1997**, *97*, 2267–2340. (e) Shanmugathasan, S.; Edwards, C.; Boyle, R. W. *Tetrahedron* **2000**, *56*, 1025–1046.

(5) (a) Curtis, N. F. *Coord. Chem. Rev.* **1968**, *3*, 3–47. (b) Kolchinski, A. G. *Coord. Chem. Rev.* **1998**, *174*, 207–239. (c) Vigato, P. A.; Tamburini, S.; Bertolo, L. *Coord. Chem. Rev.* **2007**, *251*, 1311–1492.

(6) (a) Garnovskii, A. D.; Nivorozhkin, A. L.; Minkin, V. I. *Coord. Chem. Rev.* **1993**, *126*, 1–69. (b) Sinn, E.; Harris, C. M. *Coord. Chem. Rev.* **1969**, *4*, 391–422. (c) Wezenberg, S. J.; Kleij, A. W. *Angew. Chem., Int. Ed.* **2008**, *47*, 2354–2364. (d) Kleij, A. W. *Chem.—Eur. J.* **2008**, *14*, 10520–10529.

(7) (a) Tschugaeff, L. *Chem. Ber.* **1905**, *38*, 2520–2522. (b) Godycki, L. E.; Rundle, R. E. *Acta Crystallogr.* **1953**, *6*, 487–495.

Published on Web 10/07/2009

Scheme 1. One-Pot, Template Cyclization of Tetraoxime Macrocyclic Complexes

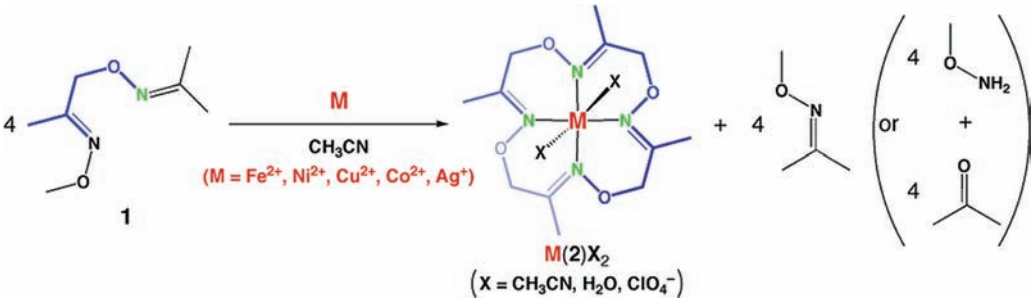

Scheme 2. Synthetic Route for Dioxime **1**[a]

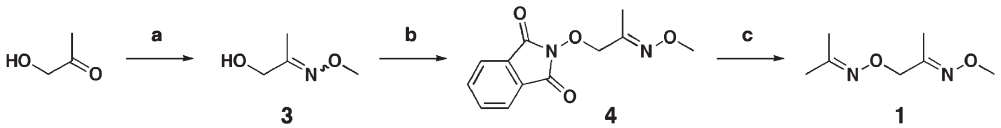

[a] Reagents and conditions: (a) $NH_2OCH_3 \cdot HCl$, Na_2CO_3, H_2O, rt, 99% (*E*/*Z* mixture); (b) (i) *N*-hydroxyphthalimide, PPh_3, DEAD, THF, rt; (ii) recrystallized from *n*-hexane and ethyl acetate, 44%; (c) (i) $NH_2NH_2 \cdot H_2O$, CH_3OH, rt; (ii) acetone, CH_3OH, rt, 94%.

examples of chemically modified dimethylglyoxime motifs have been reported.[8] More recently, other oxime motifs such as oxime-based salen-like ligands have been employed for larger macrocyclic ligands and their metal complexes with unique chemical and physical properties.[9] Herein, we report one-pot, template syntheses of a new class of metallomacrocycles with a novel 16-membered tetraoxime cyclic skeleton, $[M(\mathbf{2})X_2]Y_n$ ($M = Fe^{2+}$, Ni^{2+}, Cu^{2+}, Co^{2+}, or Ag^+), (X = axial ligand, Y = outer-sphere counteranion, $n = 0 - 2$), from dioxime **1** as a building block through continual metal-mediated oxime exchange reactions (Scheme 1). In the cyclization step, metal ions appear to play a crucial role in both activating and templating. An electrochemical study revealed that this novel ligand tends to stabilize the lower oxidation states of the included metal. Moreover, metal-free ligand **2** (3,7,11,15-tetramethyl-1,5,9,13,2,6,10,14-tetraoxa-tetraazacyclohexa-2,6,10,14-tetraene), which involves tetraoxime ether units arranged in a head-to-tail manner, was successfully prepared from dioxime **1** and Fe^{2+} via $[Fe(\mathbf{2})]^{2+}$ in an excellent yield.

Results and Discussion

Template Syntheses of Tetraoxime Macrocyclic Metal Complexes. A newly designed dioxime **1** has two -C=N−O- moieties that offer a 6-membered chelate ring as a part of N_4 macrocyclic structure. The pure *E*-isomer of dioxime **1** was synthesized from acetol in three steps in 41% overall yield (Scheme 2).

Among transition-metal ions examined for complexation with **1**, Fe^{2+}, Ni^{2+}, Cu^{2+}, Co^{2+}, and Ag^+ ions produced mononuclear metal complexes with a macrocyclic tetraaza ligand formed as a result of four-component oxime condensation. For instance, the reaction of **1** with 0.25 equiv of $Fe(ClO_4)_2 \cdot 6H_2O$ in CH_3CN at 60 °C for 13 h afforded a mononuclear Fe^{2+} complex with a 16-membered N_4 macrocyclic ligand **2**, $[Fe(\mathbf{2})(CH_3CN)_2](ClO_4)_2$, as red purple block crystals in 69% isolated yield. The same reaction followed by the removal of Fe^{2+} gave a metal-free ligand **2** in 90% yield, as mentioned later. This suggests that the one-pot cyclization by four dioxime **1** proceeded very efficiently through continual oxime exchange reactions. Other mononuclear Ni^{2+} and Cu^{2+} complexes, $[Ni(\mathbf{2})(H_2O)_2](ClO_4)_2$ and $Cu(\mathbf{2})(ClO_4)_2$, were also obtained in 36% and 24% yields, respectively, by the reactions of **1** with $Ni(ClO_4)_2 \cdot 6H_2O$ or $Cu(ClO_4)_2 \cdot 6H_2O$ under similar conditions. The formation of these complexes in CH_3CN was confirmed by electrospray ionization-time-of-flight (ESI-TOF) mass spectrometry (*m*/*z* 439.0 $[Fe(\mathbf{2})ClO_4]^+$, 441.0 $[Ni(\mathbf{2})ClO_4]^+$, and 445.9 $[Cu(\mathbf{2})ClO_4]^+$, respectively: see Figures S1−S3). In addition, the formation of $[Co(\mathbf{2})]^{2+}$ and $[Ag(\mathbf{2})]^+$ by the reactions of **1** with $Co(ClO_4)_2 \cdot 6H_2O$ or $AgClO_4$ under similar conditions was also detected by ESI-TOF mass

(8) (a) Murmann, R. K. *J. Am. Chem. Soc.* **1957**, *79*, 521–526. (b) Mathur, N. K.; Narang, C. K. *Talanta* **1964**, *11*, 647–664. (c) Uhlig, E.; Friedrich, M. *Z. Anorg. Allg. Chem.* **1966**, *343*, 299–307. (d) Schrauzer, G. N.; Windgassen, R. J. *J. Am. Chem. Soc.* **1966**, *88*, 3738–3743. (e) Dreos, R.; Tauzher, G.; Costa, G.; Green, M. *J. Chem. Soc., Dalton Trans.* **1975**, 2329–2332. (f) Duda, A. M.; Karaczyn, A.; Kozłowski, H.; Fritsky, I. O.; Głowiak, T.; Prisyazhnaya, E. V.; Sliva, T. Y.; Świątek-Kozłowska, J. *J. Chem. Soc., Dalton Trans.* **1997**, 3853–3859. (g) Ahsen, V.; Gökçeli, F.; Bekâroğlu, Ö. *J. Chem. Soc., Dalton Trans.* **1987**, 1827–1831.

(9) (a) Okawa, H.; Tokii, T.; Muto, Y.; Kida, S. *Bull. Chem. Soc. Jpn.* **1973**, *46*, 2464–2467. (b) Khanra, S.; Weyhermller, T.; Bill, E.; Chaudhuri, P. *Inorg. Chem.* **2006**, *45*, 5911–5923. (c) Akine, S.; Taniguchi, T.; Nabeshima, T. *Chem. Lett.* **2001**, 682–683. (d) Akine, S.; Taniguchi, T.; Nabeshima, T. *Angew. Chem., Int. Ed.* **2002**, *41*, 4670–4673. (e) Akine, S.; Taniguchi, T.; Saiki, T.; Nabeshima, T. *J. Am. Chem. Soc.* **2005**, *127*, 540–541. (f) Akine, S.; Kagiyama, S.; Nabeshima, T. *Inorg. Chem.* **2007**, *46*, 9525–9527. (g) Akine, S.; Sunaga, S.; Taniguchi, T.; Miyazaki, H.; Nabeshima, T. *Inorg. Chem.* **2007**, *46*, 2959–2961. (h) Veggel, F. C. J. M.; Harkema, S.; Bos, M.; Verboom, W.; Woolthuis, G. K.; Reinhoudt, D. N. *J. Org. Chem.* **1989**, *54*, 2351–2359.

(10) A mixture of Pd^{2+} and dioxime **1** preferentially produced a 1:2 square-planar complex $[Pd(\mathbf{1})_2]^{2+}$ (see the figure below), and its coordination structure was preliminarily determined by X-ray analysis. Such a structure may be one of the possible intermediates in the conversion of dioxime **1** to the final products formed in each metal-mediated reaction.

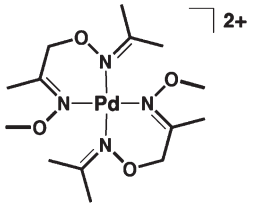

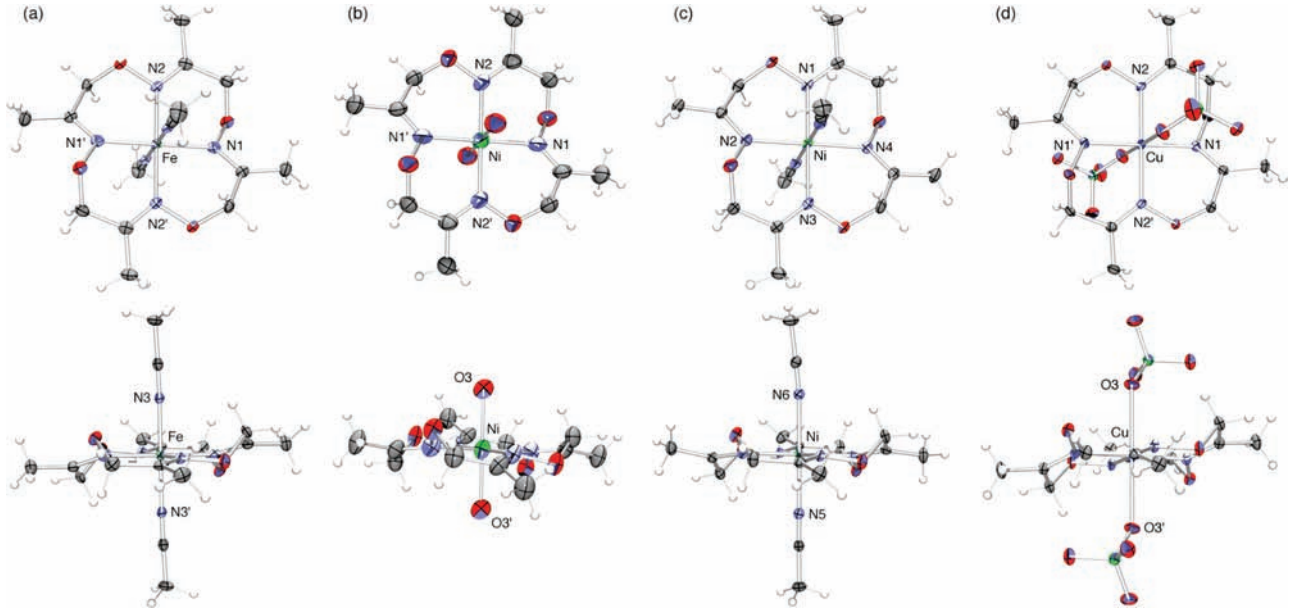

Figure 1. Crystal structures of (a) $[Fe(\mathbf{2})(CH_3CN)_2]^{2+}$, (b) $[Ni(\mathbf{2})(H_2O)_2]^{2+}$, (c) $[Ni(\mathbf{2})(CH_3CN)_2]^{2+}$, and (d) $Cu(\mathbf{2})(ClO_4)_2$. Molecular structures are represented with 50% thermal ellipsoids and viewed from the top (top) and the side (bottom). For clarity, ClO_4^- anions are omitted in the cases of Fe^{2+} and Ni^{2+} complexes.

Scheme 3. Schematic Representation of Metal-Mediated Formation of M(**2**) from **1** through Oxime Exchange Reactions

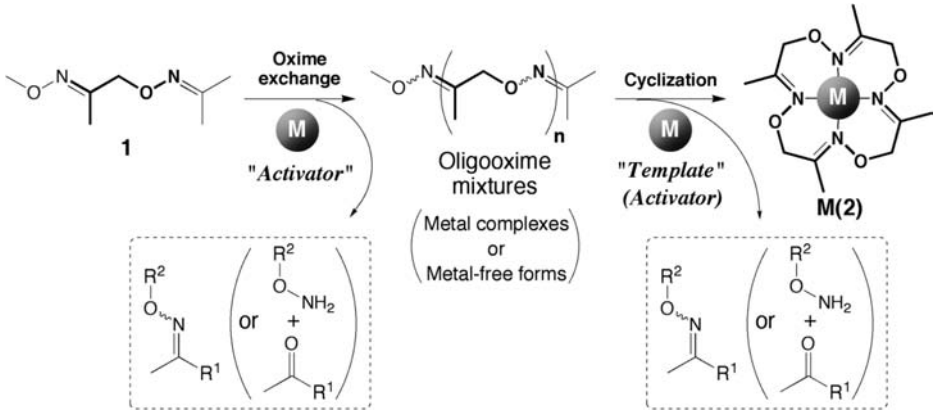

(m/z 442.1 $[Co(\mathbf{2})ClO_4]^+$ and 391.0 $[Ag(\mathbf{2})]^+$, respectively: see Figures S5 and S6).

To reveal the roles of metal ions in the one-pot cyclization, the cyclization reaction was monitored by ESI-TOF mass. In an early stage of the reactions of **1** and Fe^{2+}, Ni^{2+}, Cu^{2+}, Co^{2+}, or Ag^+, we observed the formation of linear oligooxime mixtures generated through oxime exchange reactions of several dioxime **1**.[10] Then, tetraoxime macrocyclic metal complexes gradually appeared (Figure S7). Therefore, these metal ions were believed to function as both an activator for oxime exchange reactions and a template for cyclization (Scheme 3). In contrast, similar reactions of $CuPF_6\cdot(CH_3CN)_4$ or $Zn(ClO_4)_2\cdot 6H_2O$ with **1** did not afford any macrocyclic products but linear oligooxime mixtures only. This result suggests that Cu^+ and Zn^{2+} ions act only as activators for oxime exchange reactions under the similar condition. Thus, this cyclization reaction is metal-dependent.

Interestingly, the continual oxime exchange reaction promoted not only the formation of macrocyclic tetraoxime but also the reduction of metal ions. For instance, the reaction of ferric $Fe(ClO_4)_3\cdot 6H_2O$ with **1** afforded the ferrous macrocyclic complex, $[Fe(\mathbf{2})]^{2+}$, which was identical to $[Fe(\mathbf{2})(CH_3CN)_2](ClO_4)_2$ prepared from ferrous $Fe(ClO_4)_2\cdot 6H_2O$. The reduction of Fe^{3+} or $[Fe(\mathbf{2})]^{3+}$ should take place under a reductive condition arising from R-O-NH_2 species which is an intermediate during the oxime exchange reaction. This phenomenon was also supported by the observation of monovalent $[Cu(\mathbf{2})]^+$ species in the ESI-TOF mass measurement during the template synthesis of $[Cu(\mathbf{2})]^{2+}$ from $Cu(ClO_4)_2\cdot 6H_2O$ (Figure S3).

Structures and Chemical Properties of Tetraoxime Macrocyclic Complexes. The molecular structures of macrocyclic complexes, $[Fe(\mathbf{2})(CH_3CN)_2](ClO_4)_2$, $[Ni(\mathbf{2})(X)_2](ClO_4)_2$ (X = H_2O or CH_3CN), and $Cu(\mathbf{2})(ClO_4)_2$, were determined by single-crystal X-ray analyses (Figure 1). These complexes have an octahedral coordination geometry with four nitrogen donor atoms of **2** in the equatorial positions and the solvent molecules/anions occupying the axial coordination sites, in which the ring conformations of **2** are similar to each other (Tables 1−4). In the crystal structure of

Table 1. Selected Bond Lengths (Å) and Angles (deg) for $[Fe(\mathbf{2})(CH_3CN)_2](ClO_4)_2$

Fe(1)−N(1)	1.953(2)	Fe(1)−N(3)	1.926(2)
Fe(1)−N(2)	1.984(2)		
N(1)−Fe(1)−N(1′)	180.00(13)	N(2)−Fe(1)−N(2′)	180.000(1)
N(1)−Fe(1)−N(2)	89.38(9)	N(2)−Fe(1)−N(3)	89.55(9)
N(1)−Fe(1)−N(2′)	90.62(9)	N(2)−Fe(1)−N(3′)	90.45(9)
N(1)−Fe(1)−N(3)	88.32(10)	N(3)−Fe(1)−N(3′)	180.00(14)
N(1)−Fe(1)−N(3′)	91.68(10)		

Table 2. Selected Bond Lengths (Å) and Angles (deg) for $[Ni(\mathbf{2})(H_2O)_2](ClO_4)_2$

Ni(1)−N(1)	2.005(7)	Ni(1)−O(3)	2.075(7)
Ni(1)−N(2)	2.049(6)		
N(1)−Ni(1)−N(1′)	180.0(4)	N(2)−Ni(1)−N(2′)	180.0(4)
N(1)−Ni(1)−N(2)	88.8(2)	N(2)−Ni(1)−O(3)	91.5(2)
N(1)−Ni(1)−N(2′)	91.2(2)	N(2)−Ni(1)−O(3′)	88.5(2)
N(1)−Ni(1)−O(3)	87.2(3)	O(3)−Ni(1)−O(3′)	180.0(3)
N(1)−Ni(1)−O(3′)	92.8(3)		

Table 3. Selected Bond Lengths (Å) and Angles (deg) for $[Ni(\mathbf{2})(CH_3CN)_2](ClO_4)_2$

Ni(1)−N(1)	2.072(2)	Ni(1)−N(4)	2.038(2)
Ni(1)−N(2)	2.053(2)	Ni(1)−N(5)	2.074(2)
Ni(1)−N(3)	2.067(2)	Ni(1)−N(6)	2.087(2)
N(1)−Ni(1)−N(2)	90.83(8)	N(2)−Ni(1)−N(6)	87.84(8)
N(1)−Ni(1)−N(3)	179.71(7)	N(3)−Ni(1)−N(4)	90.61(8)
N(1)−Ni(1)−N(4)	89.47(8)	N(3)−Ni(1)−N(5)	90.48(9)
N(1)−Ni(1)−N(5)	89.81(8)	N(3)−Ni(1)−N(6)	88.86(8)
N(1)−Ni(1)−N(6)	90.86(8)	N(4)−Ni(1)−N(5)	88.04(8)
N(2)−Ni(1)−N(3)	89.09(8)	N(4)−Ni(1)−N(6)	92.58(8)
N(2)−Ni(1)−N(4)	179.48(9)	N(5)−Ni(1)−N(6)	179.09(9)
N(2)−Ni(1)−N(5)	91.54(8)		

Table 4. Selected Bond Lengths (Å) and Angles (deg) for $Cu(\mathbf{2})(ClO_4)_2$

Cu(1)−N(1)	1.9685(14)	Cu(1)−O(3)	2.4269(18)
Cu(1)−N(2)	2.024(2)		
N(1)−Cu(1)−N(1′)	180.00(11)	N(2)−Cu(1)−N(2′)	180.00(9)
N(1)−Cu(1)−N(2)	89.33(7)	N(2)−Cu(1)−O(3)	89.49(7)
N(1)−Cu(1)−N(2′)	90.67(7)	N(2)−Cu(1)−O(3′)	90.51(7)
N(1)−Cu(1)−O(3)	89.93(6)	O(3)−Cu(1)−O(3′)	180.0
N(1)−Cu(1)−O(3′)	90.07(6)		

$[Fe(\mathbf{2})(CH_3CN)_2]^{2+}$, a Fe^{2+} ion sits in the cavity of **2** with an average in-plane Fe−N bond distance of 1.972 Å, and two CH_3CN molecules are coordinated at the axial positions of the central Fe^{2+} ion with an average distance of 1.931 Å (Figure 1a and Table 1). The relatively short Fe−N bond distances suggest the low-spin state of Fe^{2+}, because it is well-known that low-spin, N_6 octahedral Fe^{2+} complexes show similar Fe−N bond distances (1.96−1.99 Å) in contrast with those of high-spin, N_6 octahedral Fe^{2+} complexes (2.16−2.17 Å).[11] The low-spin state of $[Fe(\mathbf{2})(CH_3CN)_2]^{2+}$ in CH_3CN was confirmed by its UV−visible absorption and ^1H NMR spectra. The *d-d* absorption band of $[Fe(\mathbf{2})(CH_3CN)_2]^{2+}$ was observed at λ_{max} = 535 nm (ε = 78 M^{-1} cm^{-1}), which is comparable to those of the low-spin Fe^{2+} complexes with 14-membered N_4 macrocyclic ligand rather than similar high-spin Fe^{2+} complexes (Figure 2).[12] The normal chemical shifts of ^1H NMR signals of $[Fe(\mathbf{2})(CD_3CN)_2]^{2+}$ in CD_3CN also

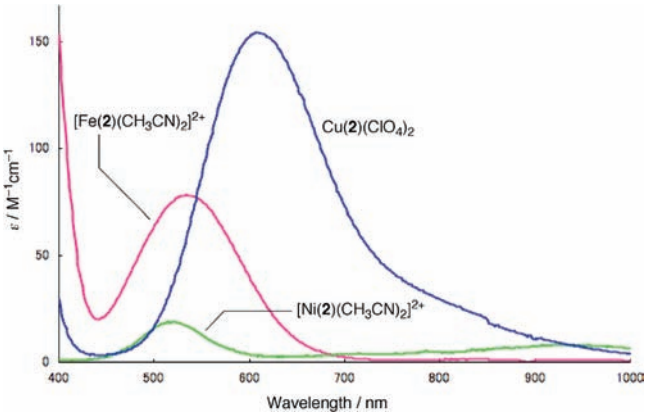

Figure 2. UV−visible absorption spectra of $[Fe(\mathbf{2})(CH_3CN)_2]^{2+}$ (31 mM, l = 0.2 cm), $[Ni(\mathbf{2})(CH_3CN)_2]^{2+}$ (1.5 mM, l = 1.0 cm), and $Cu(\mathbf{2})(ClO_4)_2$ (1.7 mM, l = 1.0 cm) in CH_3CN at 20 °C.

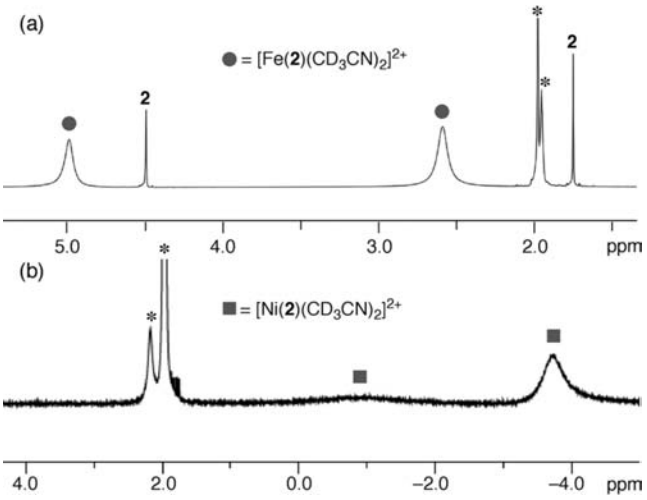

Figure 3. ^1H NMR spectra (500 MHz) of (a) $[Fe(\mathbf{2})(CD_3CN)_2]^{2+}$ (31 mM) and (b) $[Ni(\mathbf{2})(CD_3CN)_2]^{2+}$ (9 mM) in CD_3CN at 20 °C. The signals marked by an asterisk correspond to protons of solvents.

supported the existence of diamagnetic $[Fe(\mathbf{2})(CD_3CN)_2]^{2+}$ as main species (Figure 3a).[13]

As for $[Ni(\mathbf{2})]^{2+}$ complex, two H_2O or CH_3CN molecules bind to Ni^{2+} with a distance of 2.075(7) Å (Ni−O3) or distances of 2.074(2) Å (Ni−N5) and 2.087(2) Å (Ni−N6), respectively (Figures 1b,c and Tables 2 and 3). The octahedral structures of $[Ni(\mathbf{2})(H_2O)_2]^{2+}$ and $[Ni(\mathbf{2})(CH_3CN)_2]^{2+}$ with average in-plane Ni−N bond distances of 2.027 and 2.058 Å, respectively, indicate their high-spin states of Ni^{2+}. For instance, high-spin, octahedral [Ni(TAAB)I(H_2O)]I (TAAB: unsaturated 16-membered imino ligand) shows a similar average in-plane Ni−N bond distance of 2.09 Å.[14] On the other hand, low-spin, square-planar $[Ni(TAAB)](BF_4)_2$ has a shorter average in-plane Ni−N bond distance of 1.90 Å.[14] In CH_3CN, $[Ni(\mathbf{2})(CH_3CN)_2]^{2+}$ predominantly has an octahedral structure showing two *d-d* absorption bands at λ_{max} = 519 nm (ε = 19 M^{-1} cm^{-1}) and 919 nm (ε = 8 M^{-1} cm^{-1}) which are characteristic for the high-spin state (Figure 2).

(11) (a) Garcia, Y.; Kahn, O.; Rabardel, L.; Chansou, B.; Salmon, L.; Tuchagues, J. P. *Inorg. Chem.* **1999**, *38*, 4663–4670. (b) Pillet, S.; Hubsch, J.; Lecomte, C. *Eur. Phys. J. B* **2004**, *38*, 541–552. (c) Suh, Y.; Seo, M. S.; Kim, K. M.; Kim, Y. S.; Jang, H. G.; Tosha, T.; Kitagawa, T.; Kim, J.; Nam, W. *J. Inorg. Biochem.* **2006**, *100*, 627–633. (d) Johansson, L.; Molund, M.; Oskarsson, Å. *Inorg. Chim. Acta* **1978**, *31*, 117–123.

(12) Goedken, V. L.; Merrell, P. H.; Busch, D. H. *J. Am. Chem. Soc.* **1972**, *94*, 3397–3405.

(13) Due to the relatively small binding constant (ca. 8 × 10^3 M^{-1}, estimated from UV titration) of $[Fe(\mathbf{2})(CD_3CN)_2]^{2+}$ in CD_3CN, the presence of high-spin, solvated Fe^{2+} ion caused a little broadening of the signals.

(14) (a) Hawkinson, S. W.; Fleischer, E. B. *Inorg. Chem.* **1969**, *8*, 2402–2410. (b) Melson, G. A.; Busch, D. H. *J. Am. Chem. Soc.* **1964**, *86*, 4830–4833.

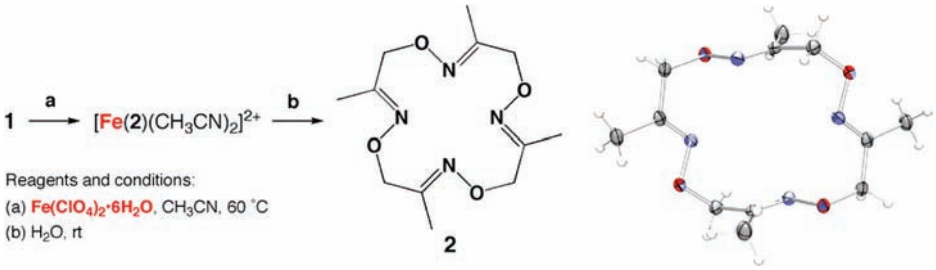

Figure 4. Schematic representation of the formation of metal-free ligand **2** via complex, $[Fe(\mathbf{2})(CH_3CN)_2]^{2+}$, and crystal structure of **2** represented with 50% thermal ellipsoids.

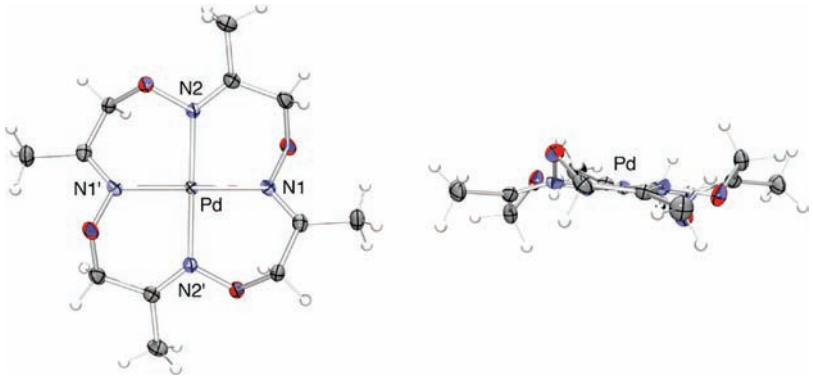

Figure 5. Crystal structures of $[Pd(\mathbf{2})]^{2+}$ represented with 50% thermal ellipsoids from the top (left) and the side (right). BF_4^- anions are omitted for clarity.

In addition, the NMR signals for $[Ni(\mathbf{2})(CH_3CN)_2]^{2+}$, that are broadened and highly upfield shifted, suggest the existence of paramagnetic Ni species (Figure 3b).

In the case of $[Cu(\mathbf{2})]^{2+}$, the in-plane Cu−N bond distances are 1.9685(14) Å (Cu−N1) and 2.024(2) Å (Cu−N2), and two ClO_4^- anions are coordinated at the axial positions of the central Cu^{2+} ion with a distance of 2.4269(18) Å (Cu−O3), indicating that this octahedral complex adopts a typical Jahn−Teller structure (Figure 1d and Table 4). Ligand field splitting energy of the $Cu(\mathbf{2})(ClO_4)_2$ was also estimated from the absorption band in CH_3CN at 608 nm ($\varepsilon = 1.5 \times 10^2$ M^{-1} cm^{-1}), which is approximately 100 nm longer compared with those of common N_4 macrocyclic Cu^{2+} complexes with saturated or unsaturated 14-membered ligands (Figure 2).[15]

The electrochemical properties of $[Fe(\mathbf{2})(CH_3CN)_2](ClO_4)_2$, $[Ni(\mathbf{2})(CH_3CN)_2](ClO_4)_2$, and $Cu(\mathbf{2})(ClO_4)_2$ were evaluated by cyclic voltammetry (CV) measurements in CH_3CN (Figures S8−S10). In the $[Fe(\mathbf{2})(CH_3CN)_2]^{2+}$ complex, the central Fe^{2+} was oxidized to Fe^{3+} ($E_{1/2} = +1.28$ V vs Ag/Ag^+), which is relatively high potential compared with similar N_4 macrocyclic Fe^{2+} complexes.[16] As for $[Ni(\mathbf{2})(CH_3CN)_2]^{2+}$ and $Cu(\mathbf{2})(ClO_4)_2$, no oxidation waves were observed in the potential window of CH_3CN, suggesting that ligand **2** stabilizes the lower oxidation states of metal ions accommodated in the cavity.[17] This tendency was also observed with large 16-membered macrocyclic complexes rather than smaller macrocycles.[3b,18]

Table 5. Selected Bond Lengths (Å) and Angles (deg) for $[Pd(\mathbf{2})](BF_4)_2$

Pd(1)−N(1)	2.001(2)	Pd(1)−N(2)	2.0147(19)
N(1)−Pd(1)−N(1′)	180.00(12)	N(1)−Pd(1)−N(2′)	91.13(8)
N(1)−Pd(1)−N(2)	88.87(8)	N(2)−Pd(1)−N(2′)	180.00(11)

Formation of Tetraoxime Metal Complexes from Metal-Free Ligand 2. We could successfully isolate tetraaza macrocyclic ligand **2** via the $[Fe(\mathbf{2})(CH_3CN)_2]^{2+}$ complex as mentioned above. A solution of dioxime **1** with $Fe(ClO_4)_2 \cdot 6H_2O$ in CH_3CN was heated at 60 °C for 2 days, followed by addition of water to remove Fe^{2+} ions from the resulting macrocycle. After a general workup, metal-free ligand **2** was isolated in 90% yield. The molecular structure of **2** was confirmed by ^1H and ^{13}C NMR spectroscopies (Figure S11) and single-crystal X-ray analysis as shown in Figure 4.

By using the metal-free ligand **2**, we could synthesize a $[Pd(\mathbf{2})]^{2+}$ complex, which could not be obtained in the one-pot cyclization of **1**. The yellow block crystals of $[Pd(\mathbf{2})](BF_4)_2$ were quantitatively prepared from the CH_3CN solution of **2** and $Pd(BF_4)_2 \cdot (CH_3CN)_4$, and characterized by single-crystal X-ray analysis (Figure 5). In contrast to other octahedral complexes, $[Pd(\mathbf{2})]^{2+}$ adopted a square-planar structure with Pd−N bond distances of 2.001(2) Å (Pd−N1) and 2.0147(19) Å (Pd−N2), corresponding to the standard geometry of N_4 macrocyclic Pd^{2+} complexes (Table 5). The formation

(15) (a) Olson, D. C.; Vasilevskis, J. *Inorg. Chem.* **1971**, *10*, 463–470. (b) Dong, Y.; Lawrance, G. A.; Lindoy, L. F.; Turner, P. *Dalton Trans.* **2003**, 1567–1576.

(16) Dabrowiak, J. C.; Lovecchio, F. V.; Goedken, V. L.; Busch, D. H. *J. Am. Chem. Soc.* **1972**, *94*, 5502–5504.

(17) In the CV measurements, a reduction wave was observed for both complexes. It is not clear yet whether this reduction takes place at the metal center or on the ligand. The details will be reported elsewhere.

(18) (a) Takvoryan, N.; Farmery, K.; Katovic, V.; Lovecchio, F. V.; Gore, E. S.; Anderson, L. B.; Busch, D. H. *J. Am. Chem. Soc.* **1974**, *96*, 731–742. (b) Fabbrizzi, L.; Poggi, A.; Zanello, P. *J. Chem. Soc., Dalton Trans.* **1983**, 2191–2195.

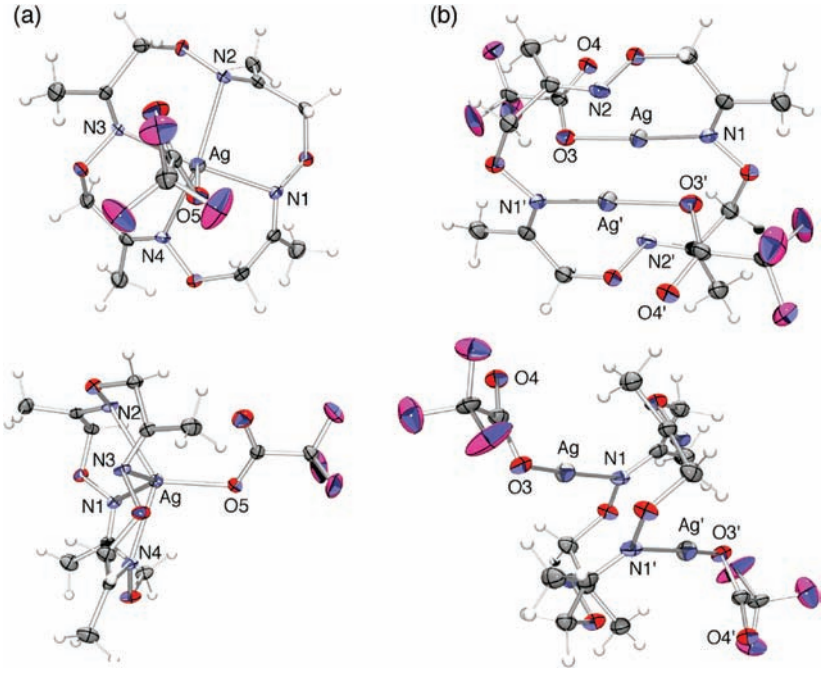

Figure 6. Crystal structures of (a) Ag(**2**)CF_3CO_2 and (b) Ag_2(**2**)$(CF_3CO_2)_2$. Molecular structures are represented with 50% thermal ellipsoids and viewed from the top (top) and the side (bottom).

Table 6. Selected Bond Lengths (Å) and Angles (deg) for Ag(**2**)CF_3CO_2

Ag(1)−N(1)	2.424(2)	Ag(1)−N(4)	2.528(2)
Ag(1)−N(2)	2.500(2)	Ag(1)−O(5)	2.305(2)
Ag(1)−N(3)	2.546(2)		
N(1)−Ag(1)−N(2)	84.70(9)	N(2)−Ag(1)−N(4)	129.75(10)
N(1)−Ag(1)−N(3)	127.48(10)	N(2)−Ag(1)−O(5)	123.51(9)
N(1)−Ag(1)−N(4)	81.37(9)	N(3)−Ag(1)−N(4)	75.06(8)
N(1)−Ag(1)−O(5)	109.40(9)	N(3)−Ag(1)−O(5)	122.06(9)
N(2)−Ag(1)−N(3)	76.12(8)	N(4)−Ag(1)−O(5)	106.65(9)

Table 7. Selected Bond Lengths (Å) and Angles (deg) for Ag_2(**2**)$(CF_3CO_2)_2$

Ag(1)−N(1)	2.219(5)	Ag(1)−O(3)	2.182(4)
N(1)−Ag(1)−O(3)	168.42(15)		

of $[Pd(\mathbf{2})]^{2+}$ in CH_3CN was also supported by ESI-TOF mass (m/z 475.9 $[Pd(\mathbf{2})BF_4]^+$: Figure S12). On the other hand, the formation of $[Fe(\mathbf{2})(CH_3CN)_2]^{2+}$, $[Ni(\mathbf{2})(CH_3CN)_2]^{2+}$, and Cu(**2**)$(ClO_4)_2$ from **2**, which were already isolated by one-pot cyclization, was also confirmed by UV−visible absorption and ESI-TOF mass spectra. For instance, a solution of **2** and $Fe(ClO_4)_2\cdot 6H_2O$ in CH_3CN immediately showed the characteristic *d-d* absorption band of $[Fe(\mathbf{2})(CH_3CN)_2]^{2+}$ at $\lambda_{max} = 535$ nm.

Finally, we found a unique coordination geometry of **2** in complexation with Ag^+, which may arise from its relatively large cavity size and structural flexibility. That is, this macrocyclic ligand **2** provided both mononuclear and dinuclear Ag^+ complexes. One is a mononuclear complex, Ag(**2**)CF_3CO_2, whose structure was determined by X-ray analysis of colorless crystals prepared from **2** and 2 equiv of $AgCF_3CO_2$ (Figure 6a). This complex has a five-coordinate, distorted square-pyramidal geometry with bond distances of 2.424(2) Å (Ag−N1), 2.500(2) Å (Ag−N2), 2.546(2) Å (Ag−N3), 2.528(2) Å (Ag−N4), and 2.305(2) Å (Ag−O5), which are common as reported for five-coordinate Ag^+ complexes (Table 6).[19] However, not lone pair but π-orbital of the N3 atom of **2** might interact with Ag^+ in Ag(**2**)CF_3CO_2 due to the irrelevant direction of the lone pair (Figure 6a). In addition to mononuclear Ag(**2**)CF_3CO_2, a dinuclear complex, Ag_2(**2**)$(CF_3CO_2)_2$, whose structure was revealed by the X-ray analysis of colorless crystals was prepared from **2** and 10 equiv of $AgCF_3CO_2$ (Figure 6b). In this structure, two nitrogen atoms of **2** independently bind to two Ag^+ ions with a distance of 2.219(5) Å, and $CF_3CO_2^-$ also coordinates to the Ag^+ ion with a distance of 2.182(4) Å, providing a typical two-coordinate, linear geometry (Table 7). Moreover, the neighboring $[Ag_2(\mathbf{2})]^{2+}$ complexes were bridged by two $CF_3CO_2^-$ anions in the crystal packing structure with Ag−Ag distances of 3.671 Å (intramacrocycle) and 4.756 Å (intermacrocycle) (Figure 7). This result indicates that the relatively large and flexible macrocycle **2** allows a one-dimensional arrangement of relatively large metal ions such as Ag^+ with the aid of bridging ligands (Figure 8).[20]

Conclusion

We have achieved a one-pot, highly efficient template synthesis of novel metal complexes, $[Fe(\mathbf{2})(CH_3CN)_2]^{2+}$, $[Ni(\mathbf{2})X_2]^{2+}$ (X = H_2O or CH_3CN), Cu(**2**)$(ClO_4)_2$, $[Co(\mathbf{2})(CH_3CN)_2]^{2+}$, and Ag(**2**)$CF_3CO_2$, with a macrocyclic tetraoxime ligand **2** through continual oxime exchange reactions. In this reaction, metal ions function as both the template for cyclization and the activator for oxime exchange. In addition, metal-free ligand **2** can be easily

(19) (a) Shi, X.-F.; Liu, H.-M.; Zhang, W.-Q. *J. Mol. Struct.* **2005**, *754*, 37–40. (b) Blake, A. J.; Champness, N. R.; Cooke, P. A.; Nicolson, J. E. B. *Chem. Commun.* **2000**, 665–666.

(20) In a preliminary study, the molecular structure of another dinuclear silver complex, $Ag_2(\mathbf{2})(ClO_4)_2$, was also revealed by X-ray analysis. This structure includes an Ag−Ag bond with a distance of 3.094 Å within the macrocycle **2**, suggesting that bridging ligands such as $CF_3CO_2^-$ and ClO_4^- allow the fine-tuning of the structures of Ag nanowires.

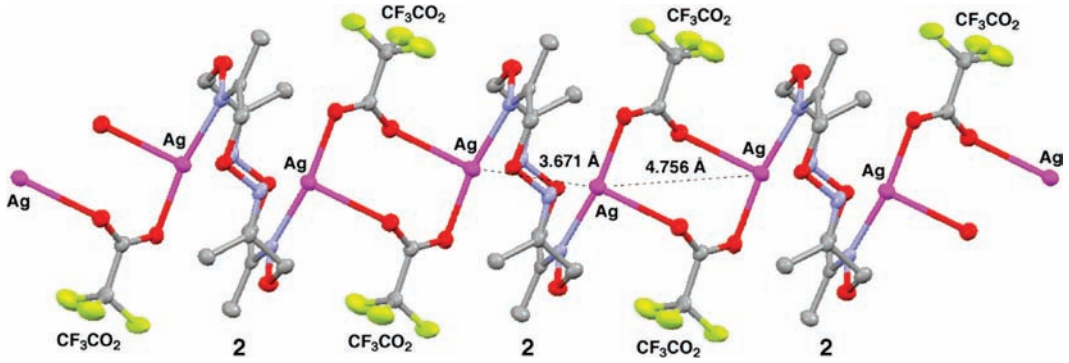

Figure 7. One-dimensional crystal packing structure of $Ag_2(\mathbf{2})(CF_3CO_2)_2$ represented with 50% thermal ellipsoids.

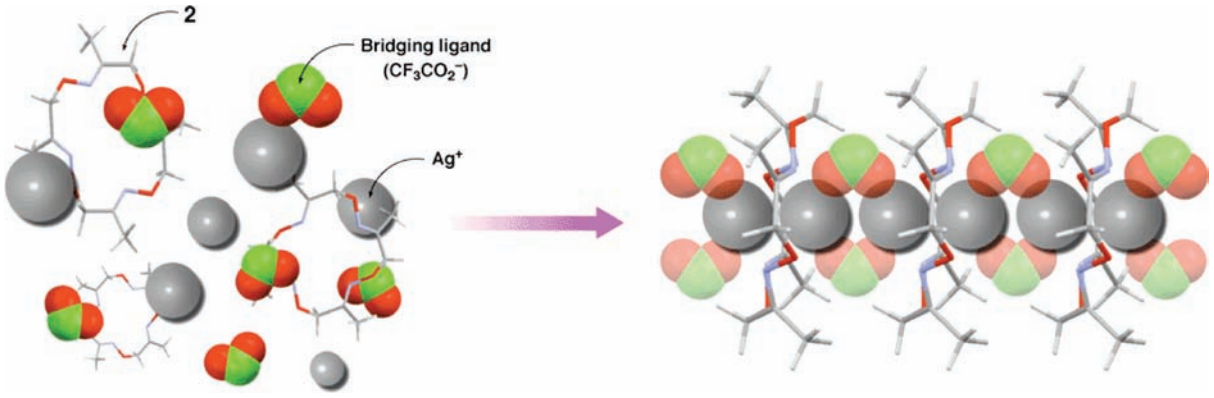

Figure 8. Schematic representation of one-dimensional arrangement of Ag^+ ions with the aid of macrocycle **2** and bridging ligands.

obtained in a high yield through this template synthesis of metal complexes. Furthermore, ligand **2** provides the $[Pd(\mathbf{2})]^{2+}$ complex, which is not obtained by the template synthesis, and two unique Ag^+ complexes, mononuclear $[Ag(\mathbf{2})]^+$ and dinuclear $[Ag_2(\mathbf{2})]^{2+}$. An electrochemical study revealed that ligand **2** tends to stabilize the lower oxidation states of metals accommodated in the cavity. Thus, the present novel macrocycle **2** allows highly efficient syntheses of a variety of macrocyclic transition-metal complexes. The chemical modification of dioxime **1** such as introduction of chirality or functional groups would allow versatile functionalization of macrocyclic ligand **2** and thereby their metal complexes. Investigation of the metal complexation of linear oligooximes is now underway.

Experimental Section

Materials and General Methods. All solvents and organic and inorganic reagents are commercially available and were used without further purification. ***Caution!*** *Although we did not encounter any difficulties, metal perchlorate salts with organic ligands and solvents are potentially explosive and should be prepared and handled in only small quantities with great care.*

NMR measurements were performed using a JEOL AL 400 spectrometer or a Bruker DRX 500 spectrometer. Electrospray ionization-time-of-flight (ESI-TOF) mass spectra were recorded on a Micromass LCT spectrometer. IR spectra were obtained with a JASCO FT/IR 4200 spectrometer using a ZnSe ATR method. UV−visible absorption spectra were recorded on a HITACHI U-3500 spectrophotometer.

Cyclic voltammetry (CV) measurements were performed in a standard cell under N_2 atmosphere equipped with a glassy carbon as a working electrode, a platinum-wire counter electrode, and an Ag^+/Ag reference electrode. The measurements were carried out in dry CH_3CN solution of n-Bu_4NClO_4 (0.1 M) purged with N_2. Scan rates (v) of 500 mV s^{-1}, 200 mV s^{-1}, and 100 mV s^{-1} were used. Working electrode was cleaned after every run.

Single-crystal X-ray crystallographic analyses were performed using a Rigaku RAXIS-RAPID imaging plate diffractometer with MoKα radiation, and obtained data were calculated using the CrystalStructure crystallographic software package except for refinement, which was performed using SHELXL-97 (Sheldrick, G. M. *SHELXL-97, Program for refinement of crystal structures*, University of Göttingen, Germany, 1997). The X-ray structures were displayed using ORTEP-3.

Synthesis of Dioxime 1. 3: To a solution of *O*-methylhydroxylamine hydrochloride (1.74 g, 20.9 mmol) in water (1.5 mL) was added a solution of sodium carbonate decahydrate (3.07 g, 10.7 mmol) in water (3 mL). A solution of hydroxyacetone (1.51 g, 20.3 mmol) in water (1.5 mL) was added to the reaction solution in a NaCl-ice bath. After stirring at room temperature for 3 h, NaCl was added to the mixture until saturated. The mixture was extracted with Et_2O (25 mL × 5), and then the combined organic phase was dried over $CaCl_2$. Evaporation of the solvent afforded **3** (2.07 g, 20.1 mmol, 99%) as a colorless oil. ^1H NMR (400 MHz, $CDCl_3$): δ 4.36 (s, 2H, CH_2), 3.87 (s, 3H, OCH_3), 1.80 (s, 3H, CH_3).

4: Compound **3** (6.02 g, 58.3 mmol), *N*-hydroxyphthalimide (9.50 g, 58.2 mmol), and PPh_3 (15.2 g, 58.0 mmol) were placed under a N_2 atmosphere in a dry flask. Dry THF (150 mL) was added to the reaction flask. To the solution was added dropwise a 40% solution of diethyl azodicarboxylate in toluene (29 mL, 63.8 mmol) at 0 °C. After stirring at room temperature for 3 h, CH_2Cl_2 (350 mL) was added to the mixture. The solution was washed with water (200 mL × 6), and the organic phase was then dried over anhydrous $MgSO_4$ and concentrated to obtain a yellow oil. The crude product was purified by silica gel column

chromatography (*n*-hexane:AcOEt = 5:1) to give an *E*/*Z* mixture of **4** (9.10 g, 36.6 mmol) as a colorless solid. Further purification was performed by recrystallization (hot *n*-hexane:AcOEt = 5:1) three times to obtain pure *E*-isomer of **4** (6.37 g, 25.7 mmol, 44% from **3**) as colorless crystals. The molecular structure of *E*-isomer of **4** was determined by X-ray single-crystal analysis (Figure S13). ^{1}H NMR (400 MHz, $CDCl_3$): δ 7.86−7.28 (m, 4H, Ar*H*), 4.63 (s, 2H, C*H*$_2$), 3.78 (s, 3H, OC*H*$_3$), 2.12 (s, 3H, C*H*$_3$). ^{13}C NMR (125 MHz, $CDCl_3$): δ 163.3, 152.2, 134.5, 128.8, 123.6, 79.0, 61.7, 12.9. IR (ATR, cm^{-1}): 1790, 1731, 1365, 1184, 1078, 1040, 987, 967, 875, 702. Mp: 104 - 105 °C. ESI-TOF MS: m/z = 249.1 as $[M + H]^+$ (calcd: 249.1). Anal. Calcd for $C_{12}H_{12}N_2O_4$: C, 58.02; H, 4.87; N, 11.29. Found: C, 57.97; H, 4.93; N, 11.28. Crystal data for *E*-isomer of **4**: $C_{12}H_{12}N_2O_4$, F_w = 248.24, crystal dimensions 0.25 × 0.13 × 0.13 mm, triclinic, space group $P\bar{1}$, a = 11.9651(7), b = 12.3116(7), c = 16.5940(8) Å, α = 89.5011(16), β = 80.3186(15), γ = 86.0787(19)°, V = 2404.0(2) Å^3, Z = 8, ρ_{calcd} = 1.372 g cm^{-3}, μ = 1.046 cm^{-1}, T = 93 K, λ(MoKα) = 0.71075 Å, $2\theta_{max}$ = 55.0°, 23830/10891 reflections collected/unique (R_{int} = 0.098), R_1 = 0.0751 ($I > 2\sigma(I)$), wR_2 = 0.2499 (for all data), GOF = 0.961, largest diff. peak and hole 0.42/−0.69 eÅ^{-3}. CCDC reference number 705238.

1: To a solution of **4** (2.00 g, 8.06 mmol) in CH_3OH (40 mL) was added hydrazine monohydrate (0.37 mL, 7.76 mmol), and the reaction mixture was then stirred at room temperature for 1 h. The suspended solution was filtered to remove insoluble white solid. The filtrate was evaporated, and the residue was dissolved into $CHCl_3$ (200 mL). The organic phase was washed with 1 M aqueous solution of sodium bicarbonate (100 mL) and dried over anhydrous $MgSO_4$. Evaporation of the solvent afforded an intermediate product possessing an acid-free amino group as a colorless oil Acetone (10 mL) was added to the solution of the intermediate in CH_3OH (40 mL), and the reaction mixture was then stirred at room temperature for 30 min. The solution was concentrated to afford an oil, which was purified by silica gel column chromatography (*n*-hexane: AcOEt = 10:1) to give **1** (1.20 g, 7.59 mmol, 94%) as a colorless oil. ^{1}H NMR (400 MHz, $CDCl_3$): δ 4.51 (s, 2H, C*H*$_2$), 3.88 (s, 3H, OC*H*$_3$), 1.88 (s, 3H, C*H*$_3$), 1.87 (s, 3H, C*H*$_3$), 1.87 (s, 3H, C*H*$_3$). ^{13}C NMR (125 MHz, $CDCl_3$): δ 155.7, 155.1, 74.3, 61.5, 21.8, 15.6, 12.0. IR (ATR, cm^{-1}): 2939, 2818, 1637, 1438, 1367, 1040, 898, 876, 826, 659. ESI-TOF MS: m/z = 181.1 as $[M + H]^+$ (calcd: 181.1). Anal. Calcd for $C_7H_{14}N_2O_2$: C, 53.15; H, 8.92; N, 17.71. Found: C, 52.92; H, 8.89; N, 17.76.

Synthesis of [Fe(2)(CH$_3$CN)$_2$](ClO$_4$)$_2$. Compound **1** (31 mg, 0.20 mmol) and $Fe(ClO_4)_2 \cdot 6H_2O$ (18 mg, 0.049 mmol) were dissolved into dry CH_3CN (0.4 mL) which was purged with N_2 in advance. The reaction mixture was heated at 60 °C for 13 h under a N_2 atmosphere in a dry flask. After addition of CH_3CN (1 mL), the solution, which was filtered to remove red brown precipitates, was evaporated, and the resulting residue was purified by recrystallization with a mixture of CH_3CN and diethyl ether to afford [Fe(**2**)(CH$_3$CN)$_2$](ClO$_4$)$_2$ (21 mg, 0.034 mmol, 69%) as red purple block crystals. ^{1}H NMR (500 MHz, 293 K, CD_3CN): δ 4.99 (brs), 2.59 (brs). ^{13}C NMR (125 MHz, 293 K, CD_3CN): δ 180.9, 71.1, 19.7. Absorption for *d*-*d* transition in CH_3CN (λ_{max}, nm; ε, M^{-1} cm^{-1}): 535 (78). IR (ATR, cm^{-1}): 3375, 3007, 2938, 2015, 1651, 1428, 1371, 1251, 1075, 1046, 975, 903, 855, 680, 659, 621. ESI-TOF MS: m/z = 439.0 as $[Fe(\mathbf{2})(ClO_4)]^+$ (calcd: 439.0). Anal. Calcd for $C_{16}H_{26}Cl_2FeN_6O_{12}$: C, 30.94; H, 4.22; N, 13.53. Found: C, 30.77; H, 4.18; N, 13.31. Crystal data for complex [Fe(**2**)(CH$_3$CN)$_2$](ClO$_4$)$_2$: $C_{16}H_{26}Cl_2FeN_6O_{12}$, F_w = 621.17, crystal dimensions 0.10 × 0.10 × 0.10 mm, monoclinic, space group $P2_1/c$, a = 15.1943(7), b = 9.6651(4), c = 17.3481(11) Å, β = 101.9473(19)°, V = 2492.5(2) Å^3, Z = 4, ρ_{calcd} = 1.655 g cm^{-3}, μ = 8.90 cm^{-1}, T = 93 K, λ(MoKα) = 0.71075 Å, $2\theta_{max}$ = 55.0°, 23746/5712 reflections collected/unique (R_{int} = 0.084), R_1 = 0.0473 ($I > 2\sigma(I)$), wR_2 = 0.1208 (for all data), GOF = 1.036, largest diff. peak and hole 0.57/−0.63 eÅ^{-3}. CCDC reference number 725064.

Synthesis of [Ni(2)X$_2$](ClO$_4$)$_2$ (X = H$_2$O or CH$_3$CN). Compound **1** (25 mg, 0.16 mmol) and $Ni(ClO_4)_2 \cdot 6H_2O$ (14 mg, 0.039 mmol were dissolved into CH_3CN (0.3 mL), and the reaction mixture was then heated at 60 °C for 6 days. After slow evaporation of the solution over 2 days, purple crystals were precipitated. The obtained crystals were collected and washed with a small amount of cold CH_3CN to obtain [Ni(**2**)(H$_2$O)$_2$](ClO$_4$)$_2$ (8.0 mg, 0.014 mmol, 36%). Recrystallization of the resulting Ni^{2+} complex from CH_3CN also afforded red purple crystals of [Ni(**2**)(CH$_3$CN)$_2$](ClO$_4$)$_2$ as a result of replacement of H_2O by CH_3CN at the axial positions. ^{1}H NMR (500 MHz, CD_3CN): δ −0.80 (brs), −3.68 (brs). Absorption for *d*-*d* transition in CH_3CN (λ_{max}, nm; ε, M^{-1} cm^{-1}): 919 (8), 519 (19). IR of [Ni(**2**)(H$_2$O)$_2$](ClO$_4$)$_2$ (ATR, cm^{-1}): 3449, 3395, 1421, 1366, 1059, 1037, 968, 930, 909, 858, 621. ESI-TOF MS: m/z = 441.0 as $[Ni(\mathbf{2})(ClO_4)]^+$ (calcd: 441.0). Anal. Calcd for $C_{12}H_{24}Cl_2N_4NiO_{14}$ {[Ni(**2**)(H$_2$O)$_2$](ClO$_4$)$_2$}: C, 24.94; H, 4.19; N, 9.69. Found: C, 24.71; H, 4.29; N, 9.41. Anal. Calcd for $C_{14}H_{23}Cl_2N_5NiO_{12}$ {[Ni(**2**)CH$_3$CN](ClO$_4$)$_2$: one CH_3CN molecule was dissociated from [Ni(**2**)(CH$_3$CN)$_2$](ClO$_4$)$_2$ through the measurement due to the labile nature of the axial CH_3CN-Ni bonds}: C, 28.84; H, 3.98; N, 12.01. Found: C, 28.69; H, 4.05; N, 11.88. Crystal data for complex [Ni(**2**)(H$_2$O)$_2$](ClO$_4$)$_2$: $C_{12}H_{24}Cl_2N_4NiO_{14}$, F_w = 577.95, crystal dimensions 0.10 × 0.02 × 0.02 mm, triclinic, space group $P\bar{1}$, a = 7.496(4), b = 8.246(4), c = 9.762(5) Å, α = 85.102(11), β = 71.776(11), γ = 70.187(11)°, V = 539.1(4) Å^3, Z = 1, ρ_{calcd} = 1.780 g cm^{-3}, μ = 12.26 cm^{-1}, T = 93 K, λ(MoKα) = 0.71075 Å, $2\theta_{max}$ = 55.0°, 5347/2466 reflections collected/unique (R_{int} = 0.097), R_1 = 0.0954 ($I > 2\sigma(I)$), wR_2 = 0.2693 (for all data), GOF = 1.063, largest diff. peak and hole 0.98/−1.62 eÅ^{-3}. CCDC reference number 725065. Crystal data for complex [Ni(**2**)(CH$_3$CN)$_2$](ClO$_4$)$_2$: $C_{16}H_{26}Cl_2N_6NiO_{12}$, F_w = 624.02, crystal dimensions 0.35 × 0.25 × 0.20 mm, monoclinic, space group $P2_1$, a = 7.7332(3), b = 9.6883(5), c = 17.3374(8) Å, β = 103.7653(17)°, V = 1261.63(11) Å^3, Z = 2, ρ_{calcd} = 1.643 g cm^{-3}, μ = 10.51 cm^{-1}, T = 93 K, λ(MoKα) = 0.71075 Å, $2\theta_{max}$ = 55.0°, 12450/5632 reflections collected/unique (R_{int} = 0.022), R_1 = 0.0294 ($I > 2\sigma(I)$), wR_2 = 0.0740 (for all data), GOF = 1.030, largest diff. peak and hole 0.54/−0.37 eÅ^{-3}. CCDC reference number 705236.

Synthesis of Cu(2)(ClO$_4$)$_2$. Compound **1** (66 mg, 0.42 mmol) and $Cu(ClO_4)_2 \cdot 6H_2O$ (39 mg, 0.104 mmol) were dissolved into CH_3CN (2 mL), and the reaction mixture was then heated at reflux for 10 h. After evaporation, the residue was purified by recrystallization with a mixture of CH_3CN and diethyl ether. Obtained crystals were dissolved into CH_3CN and insoluble material was filtered off. After evaporation, the residue was recrystallized from hot CH_3CN three times to afford Cu(**2**)-(ClO$_4$)$_2$ (13.6 mg, 0.0249 mmol, 24%) as purple block crystals. Unidentified green-colored crystals could be removed by hand. The low yield in the case of Cu^{2+} is ascribable to the reduction of Cu^{2+} into nontemplate Cu^+ during the reaction. ^{1}H NMR (500 MHz, CD_3CN): δ −2.62 (brs). Absorption for *d*-*d* transition in CH_3CN (λ_{max}, nm; ε, M^{-1} cm^{-1}): 608 (150). IR (ATR, cm^{-1}): 2979, 2919, 1650, 1424, 1366, 1106, 1046, 976, 619. ESI-TOF MS: m/z = 445.9 as $[Cu(\mathbf{2})(ClO_4)]^+$ (calcd: 446.0). Anal. Calcd for $C_{12}H_{20}Cl_2CuN_4O_{12}$: C, 26.36; H, 3.69; N, 10.25. Found: C, 26.19; H, 3.69; N, 9.99. Crystal data for complex [Cu(**2**)](ClO$_4$)$_2$: $C_{12}H_{20}Cl_2CuN_4O_{12}$, F_w = 546.76, crystal dimensions 0.22 × 0.08 × 0.02 mm, triclinic, space group $P\bar{1}$, a = 6.9994(3), b = 8.2518(4), c = 9.4228(4) Å, α = 89.3329(14), β = 71.5254(14), γ = 74.8919(15)°, V = 496.85(4) Å^3, Z = 1, ρ_{calcd} = 1.827 g cm^{-3}, μ = 14.396 cm^{-1}, T = 133 K, λ(MoKα) = 0.71075 Å, $2\theta_{max}$ = 55.0°, 8551/2261 reflections collected/unique (R_{int} = 0.022), R_1 = 0.0250 ($I > 2\sigma(I)$), wR_2 = 0.0683 (for all data), GOF = 1.223, largest diff. peak and hole 0.49/−0.48 eÅ^{-3}. CCDC reference number 705235.

Synthesis of [Fe(2)(CH$_3$CN)$_2$](ClO$_4$)$_2$ from 1 and Fe^{3+}. Compound **1** (15 mg, 0.095 mmol) and $Fe(ClO_4)_3 \cdot 6H_2O$ (11 mg, 0.024 mmol) were dissolved into dry CH_3CN (0.1 mL) which was purged with N_2 in advance. The reaction mixture was

heated at 70 °C for 24 h under a N_2 atmosphere in a dry flask. After addition of CH_3CN (3 mL), the solution, which was filtered to remove insoluble material, was evaporated, and the resulting residue was purified by recrystallization with CH_3CN or a mixture of CH_3CN and diethyl ether to afford red crystals. X-ray analysis revealed that the obtained crystal was the ferrous complex, $[Fe(\mathbf{2})(CH_3CN)_2](ClO_4)_2$. Its ^1H NMR spectral pattern in CD_3CN was consistent with that of $[Fe(\mathbf{2})(CH_3CN)_2]^{2+}$ in the low-spin state separately prepared from Fe^{2+} and **1**.

Synthesis of Macrocyclic Ligand 2 via Fe^{2+} Complex. Compound **1** (28 mg, 0.18 mmol) and $Fe(ClO_4)_2 \cdot 6H_2O$ (15 mg, 0.041 mmol) were dissolved into dry CH_3CN (0.35 mL) which was purged with N_2 in advance. The reaction mixture was heated at 60 °C for 1 day under a N_2 atmosphere in a dry flask. After evaporation of the solvent, the residue was poured into water (4 mL) and extracted with CH_2Cl_2 (6 mL × 3). The organic layers were combined, dried over anhydrous $MgSO_4$, and evaporated. The resulting residue was purified by silica gel column chromatography (AcOEt) to afford **2** (10.6 mg, 0.037 mmol, 90%). Further purification was performed by recrystallization from hot toluene to obtain **2** as colorless block crystals. ^1H NMR (500 MHz, $CDCl_3$): δ 4.57 (s, 8H, CH_2), 1.82 (s, 12H, CH_3). ^{13}C NMR (125 MHz, $CDCl_3$): δ 155.9, 73.4, 11.7. IR (ATR, cm^{-1}): 2960, 2925, 2853, 1731, 1643, 1426, 1362, 1091, 1036, 948, 877, 827, 678, 637. Mp.: 187−189 °C. HRMS (ESI-TOF) m/z: $[M + Na]^+$ calcd for $C_{12}H_{20}N_4O_4Na$ 307.1382, found 307.1375. Anal. Calcd for $C_{12}H_{20}N_4O_4$: C, 50.69; H, 7.09; N, 19.71. Found: C, 50.77; H, 7.07; N, 19.64. Crystal data for **2**: $C_{12}H_{20}N_4O_4$, $F_w = 284.31$, monoclinic, space group $P2_1/c$, $a = 8.1968(4)$, $b = 9.3192(5)$, $c = 9.6427(6)$ Å, $\beta = 95.0169(18)°$, $V = 733.76(7)$ Å^3, $Z = 2$, $\rho_{calcd} = 1.287$ g cm^{-3}, $\mu = 0.977$ cm^{-1}, $T = 133$ K, λ(MoKα) = 0.71075 Å, $2\theta_{max} = 55.0°$, 11905/1674 reflections collected/unique ($R_{int} = 0.015$), $R_1 = 0.0380$ ($I > 2\sigma(I)$), $wR_2 = 0.1130$ (for all data), GOF = 1.104, largest diff. peak and hole 0.32/−0.33 eÅ^{-3}. CCDC reference number 705237.

Synthesis of $[Pd(\mathbf{2})](BF_4)_2$ from Metal-Free Ligand 2. Metal-free ligand **2** (2.8 mg, 9.8 μmol) and $Pd(BF_4)_2 \cdot (CH_3CN)_4$ (5.1 mg, 11.5 μmol) were dissolved into CD_3CN (0.6 mL), and the reaction mixture was then allowed to stand for 2 days at room temperature. The crude solution was evaporated, and the resulting residue was purified by recrystallization with a mixture of CH_3CN and diethyl ether to afford $[Pd(\mathbf{2})](BF_4)_2$ (5.9 mg, 10 μmol, quant.) as yellow block crystals. ^1H NMR (500 MHz, 293 K, CD_3CN): δ 4.99 (s), 2.39 (s). ^{13}C NMR (125 MHz, 293 K, CD_3CN): δ 171.5, 74.3, 19.9. IR (ATR, cm^{-1}): 2922, 2851, 2254, 1632, 1425, 1372, 1287, 1032, 923, 868, 766, 670, 656. ESI-TOF MS: $m/z = 475.9$ as $[Pd(\mathbf{2})(BF_4)]^+$ (calcd: 476.1). Anal. Calcd for $C_{12}H_{20}B_2F_8N_4O_4Pd$: C, 25.54; H, 3.57; N, 9.93. Found: C, 25.65; H, 3.70; N, 10.05. Crystal data for complex $[Pd(\mathbf{2})](BF_4)_2$: $C_{12}H_{20}B_2F_8N_4O_4Pd$, $F_w = 564.32$, crystal dimensions 0.25 × 0.15 × 0.15 mm, monoclinic, space group $P2_1/n$, $a = 6.5309(6)$, $b = 14.0356(10)$, $c = 11.1689(8)$ Å, $\beta = 101.131(3)°$, $V = 1000.38(14)$ Å^3, $Z = 2$, $\rho_{calcd} = 1.873$ g cm^{-3}, $\mu = 10.29$ cm^{-1}, $T = 93$ K, λ(MoKα) = 0.71075 Å, $2\theta_{max} = 55.0°$, 9389/2283 reflections collected/unique ($R_{int} = 0.035$), $R_1 = 0.0280$ ($I > 2\sigma(I)$), $wR_2 = 0.0676$ (for all data), GOF = 1.147, largest diff. peak and hole 0.75/−0.66 eÅ^{-3}. CCDC reference number 725066.

Synthesis of Mononuclear $Ag(\mathbf{2})CF_3CO_2$ from Metal-Free Ligand 2. Metal-free ligand **2** (0.8 mg, 2.8 μmol) and $AgCF_3CO_2$ (1.3 mg, 5.7 μmol) were dissolved into CH_3CN (0.5 mL), and the reaction mixture was then allowed to stand for 1 day at room temperature in the dark. After slow evaporation of the solvent, colorless crystals were obtained. Crystal data for complex $Ag(\mathbf{2})CF_3CO_2$: $C_{14}H_{20}AgF_3N_4O_6$, $F_w = 505.20$, crystal dimensions 0.22 × 0.10 × 0.10 mm, monoclinic, space group $P2_1/n$, $a = 10.1993(4)$, $b = 13.2126(6)$, $c = 14.5055(8)$ Å, $\beta = 103.2141(15)°$, $V = 1902.99(15)$ Å^3, $Z = 4$, $\rho_{calcd} = 1.763$ g cm^{-3}, $\mu = 11.24$ cm^{-1}, $T = 93$ K, λ(MoKα) = 0.71075 Å, $2\theta_{max} = 55.0°$, 17729/4362 reflections collected/unique ($R_{int} = 0.072$), $R_1 = 0.0430$ ($I > 2\sigma(I)$), $wR_2 = 0.0975$ (for all data), GOF = 1.050, largest diff. peak and hole 0.71/−1.48 eÅ^{-3}. CCDC reference number 725067.

Synthesis of Dinuclear $Ag_2(\mathbf{2})(CF_3CO_2)_2$ from Metal-Free Ligand 2. Metal-free ligand **2** (0.6 mg, 2.1 μmol) and $AgCF_3CO_2$ (4.6 mg, 21 μmol) were dissolved into a mixture of CH_3CN (0.2 mL) and toluene (0.2 mL), and the reaction mixture was then allowed to stand for 4 h at room temperature in the dark. After slow evaporation of the solvents, colorless plate crystals appeared with a lot of microcrystals. The microcrystals are probably excess $AgCF_3CO_2$ because of the amount and shape of the crystals. The plate crystal was analyzed by X-ray analysis. Crystal data for complex $Ag_2(\mathbf{2})(CF_3CO_2)_2$: $C_{16}H_{20}Ag_2F_6N_4O_8$, $F_w = 726.08$, crystal dimensions 0.28 × 0.20 × 0.10 mm, monoclinic, space group $P2_1/c$, $a = 7.7688(8)$, $b = 19.714(2)$, $c = 8.2951(11)$ Å, $\beta = 117.297(3)°$, $V = 1128.9(2)$ Å^3, $Z = 2$, $\rho_{calcd} = 2.136$ g cm^{-3}, $\mu = 18.31$ cm^{-1}, $T = 93$ K, λ(MoKα) = 0.71075 Å, $2\theta_{max} = 55.0°$, 10898/2579 reflections collected/unique ($R_{int} = 0.062$), $R_1 = 0.0480$ ($I > 2\sigma(I)$), $wR_2 = 0.1190$ (for all data), GOF = 1.173, largest diff. peak and hole 1.21/−1.41 eÅ^{-3}. CCDC reference number 725068.

Acknowledgment. We thank Prof. H. Nishihara and Dr. S. Muratsugu for their kind help in the CV measurements. We are grateful to Ms. J. Han for some preliminary experiments. This study was supported by the Global COE Program for Chemistry Innovation through Cooperation of Science and Engineering and a Grant-in-Aid for Scientific Research (S) to M.S. (Grant No. 16105001) from the Ministry of Education, Culture, Sports, Science and Technology of Japan.

Supporting Information Available: ESI-TOF mass, NMR and CV spectra, and X-ray crystallographic data of complexes $[Fe(\mathbf{2})(CH_3CN)_2](ClO_4)_2$, $[Ni(\mathbf{2})(H_2O)_2](ClO_4)_2$, $[Ni(\mathbf{2})(CH_3CN)_2](ClO_4)_2$, $Cu(\mathbf{2})(ClO_4)_2$, $[Pd(\mathbf{2})](BF_4)_2$, $Ag(\mathbf{2})CF_3CO_2$, $Ag_2(\mathbf{2})(CF_3CO_2)_2$, and ligand **2** in CIF format. This material is available free of charge via the Internet at http://pubs.acs.org.